Thermo-Hydraulic State Estimation and Robust Decision Support for Multiphase Kick Transients from Sparse Surface Measurements

Juan Esteban Cárdenas[1], **Mateo Andrés Villalba**[2], **and Santiago Ricardo Borrero**[3]
[1]Universidad de Pamplona, Calle 28B 14–67, Barrio Miraflores, Pamplona, Norte de Santander, Colombia
[2]Universidad Surcolombiana, Carrera 9A 22–41, Sector La Merced, Neiva, Huila, Colombia
[3]Corporación Universitaria del Caribe (CECAR), Avenida Los Fundadores 5–118, Urbanización El Prado, Sincelejo, Sucre, Colombia

ABSTRACT Early identification and characterization of gas influx events during drilling remains difficult because the most reliable measurements are typically available at the surface, while the hazardous dynamics occur along an extended, heterogeneous wellbore. Surface pressure and flow signals are continuously accessible, but they are often non-unique with respect to downhole states because multiphase slip, compressibility, dissolution, and evolving frictional losses can produce similar signatures for distinct influx scenarios. This paper develops a physics-first estimation and decision-support framework that converts sparse surface measurements into probabilistic downhole reconstructions suitable for real-time operational guidance. The core contribution is a coupled thermo-hydraulic model that accounts for gas compressibility, transient annular hydraulics, and pressure- and temperature-dependent gas solubility in non-aqueous drilling fluids, embedded within a constrained moving-horizon inference scheme. The estimator jointly reconstructs the latent state fields and an unknown influx boundary profile while enforcing mass conservation, momentum balance, and phase-equilibrium consistency. To improve robustness under model-form uncertainty and unmodeled flow-regime effects, the framework augments deterministic inversion with ensemble-based uncertainty propagation and risk-calibrated decision metrics that remain meaningful when the inverse problem is ill-conditioned. Numerical experiments spanning circulating and shut-in conditions demonstrate that the method can separate competing explanations for similar surface pressure traces by exploiting the joint evolution of pressure gradient, dissolved-gas inventory, and annular holdup. The resulting system offers a principled route to rapid, quantitatively interpretable kick assessment without relying on bespoke flow-pattern labels, while remaining compatible with data-driven components as optional accelerators rather than as primary arbiters of physical plausibility.

KEYWORDS

1. Introduction

Multiphase influx events in drilling are operationally critical because they couple fast transients, strong nonlinearity, and limited observability [1]. The same surface pressure deviation can arise from distinct combinations of downhole gas holdup, compressibility-driven expansion, changes in effective density, altered friction factor, or dissolution-driven buffering. When the annulus contains evolving gas structures, the pressure gra-

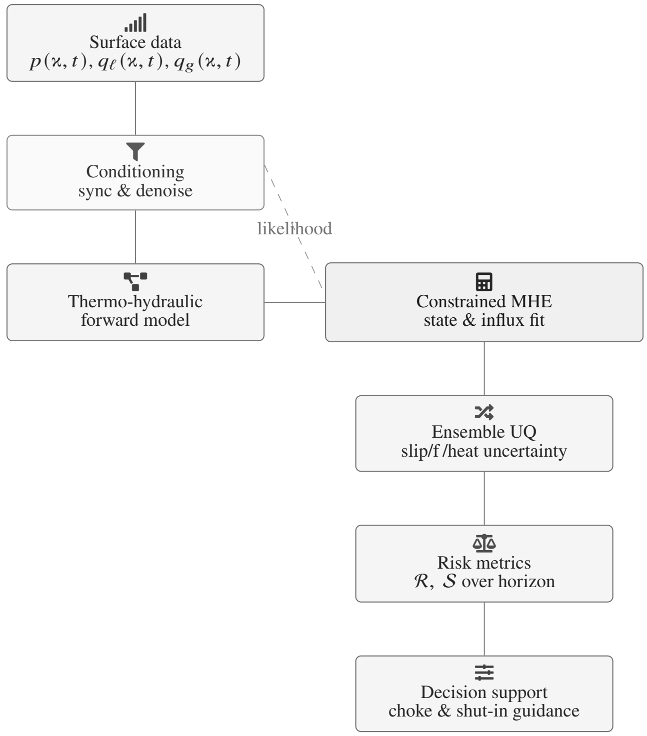

Figure 1 End-to-end estimation and decision pipeline: sparse surface measurements are conditioned and interpreted through a solubility-aware thermo-hydraulic forward model within a constrained moving-horizon estimator; ensemble uncertainty propagation yields risk-calibrated metrics used to rank operational responses.

dient becomes path-dependent and regime-sensitive, while the available measurements are often aggregated through chokes, standpipe dynamics, and sensor filtering. This creates a characteristic inverse problem: infer a distributed state and an unknown boundary disturbance from a small number of noisy measurements, under uncertain constitutive closures [2].

A pragmatic response has been to treat the mapping from surface signals to downhole regimes as a classification problem. That direction can be valuable for rapid flagging, particularly when the measurement conditions match those in training data. Under circulating conditions, machine-learning models have been shown to associate measured surface pressure and flow information with annular flow patterns at high accuracy; for example, decision-tree classification achieved reported accuracies of 96% for air influx and 98% for carbon-dioxide influx in laboratory-scale dynamic experiments, indicating that informative structure exists in surface data even when downhole dynamics are complex [3]. However, classification alone does not answer the more operational questions: How large is the influx? Where is the gas located? How much is dissolved versus free? What is the predicted near-future surface pressure trajectory under candidate choke actions? Those questions demand a quantitative state estimate together with uncertainty that reflects non-uniqueness [4].

This paper argues that the most durable path to such quantitative answers is a physically constrained inverse formulation that treats surface measurements as partial observations of a distributed conservation-law system. The thesis is not that purely mechanistic simulators are sufficient, but that mechanistic constraints are essential to prevent the estimator from proposing states that are inconsistent with mass balance, thermodynamics, or momentum coupling. In particular, two features are emphasized. First, the thermodynamic partitioning of gas between dissolved and free phases can materially alter both pit gain and pressure response by buffering the free-gas volume, especially in synthetic or non-aqueous fluids where solubility can be significant [5]. Second, the inverse problem must be posed so that it remains well-defined even when flow-regime transitions and slip closures are only approximately represented.

The main technical contribution is a coupled thermo-hydraulic model and inference scheme designed for sparse measurements. The forward model combines one-dimensional annular transport with compressible gas dynamics and a pressure- and temperature-dependent solubility relation, producing a state vector that includes pressure, phase holdups, velocities, temperature, and dissolved-gas inventory [6]. The inverse problem reconstructs both the state trajectory and an unknown influx boundary profile using moving-horizon estimation with inequality constraints and regularization designed to encode operational plausibility. A second contribution is the introduction of risk-calibrated decision metrics that transform posterior state ensembles into actionable quantities, such as the probability that gas holdup at the shoe exceeds a threshold within a lookahead horizon, or the probability that a proposed choke schedule violates a casing pressure constraint.

The framework is intended to complement, not replace, data-driven detectors. The estimation architecture accepts any auxiliary detector as an external cue or prior, but it does not

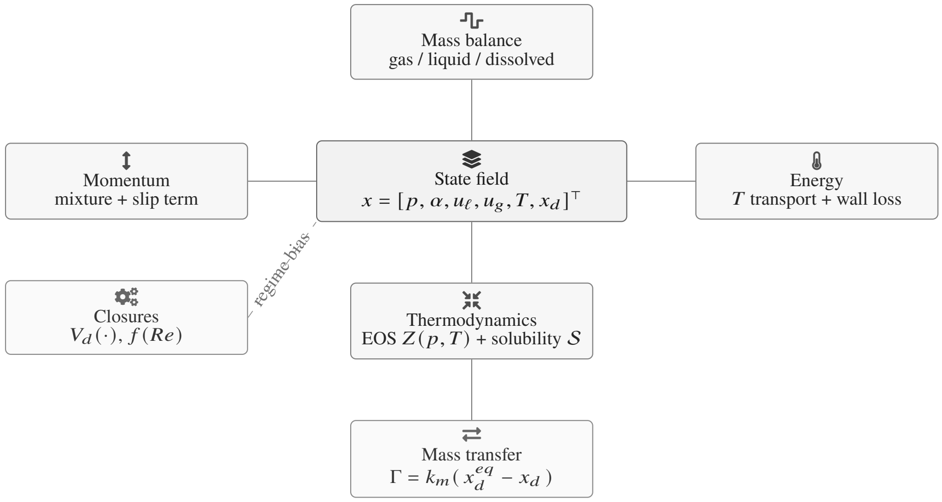

Figure 2 Coupled thermo-hydraulic structure: conservation laws evolve the distributed state, while thermodynamics (EOS and pressure/temperature-dependent solubility) and finite-rate mass transfer govern the partitioning between dissolved and free gas; closures for slip and friction enter as compact, tunable components.

require flow-pattern labels [7]. This separation matters because labels can be ambiguous, while conservation constraints are not. The remainder of the paper develops the problem formulation, the thermo-hydraulic and solubility model, the moving-horizon inversion machinery, the uncertainty-aware decision logic, and numerical experiments that illustrate how the method distinguishes physically distinct scenarios that are superficially similar at the surface.

2. Problem Formulation and Observability Structure

Consider a wellbore annulus parameterized by measured depth coordinate $z \in [\varkappa, L]$, with $z = \varkappa$ at the wellhead and $z = L$ near the influx zone. Let $t \geq \varkappa$ denote time [8]. The drilling fluid is modeled as a carrier liquid with density $\rho_\ell(p,T)$ and viscosity $\mu_\ell(p,T)$, potentially non-Newtonian in detail but represented here through an effective viscosity closure. Gas exists as a free phase with density $\rho_g(p,T)$ and as a dissolved component within the liquid characterized by a mass fraction $x_d(z,t)$. The free-gas volumetric fraction (void fraction) is $\alpha(z,t)$, the liquid fraction is $-\alpha(z,t)$, and the superficial velocities are $u_\ell(z,t)$ and $u_g(z,t)$, with a mixture velocity $u_m = \alpha u_g + (-\alpha)u_\ell$. The cross-sectional area $A(z)$ and hydraulic diameter $D_h(z)$ are assumed known from geometry [9].

The measurement model is intentionally sparse. Let the available data stream be $y(t)$ consisting of surface pressure and, optionally, surface flow rate and density estimates from mud logging. A representative measurement vector is [10]

$$y(t) = \begin{bmatrix} p(\varkappa,t) \\ q_\ell(\varkappa,t) \\ q_g(\varkappa,t) \end{bmatrix} + \eta(t), \tag{1}$$

where $q_\ell = A(-\alpha)u_\ell$ and $q_g = A\alpha u_g$ at the wellhead, and $\eta(t)$ models sensor noise and unmodeled dynamics. In many operations, only $p(\varkappa,t)$ is reliable at high frequency, with flow information delayed or filtered; the framework remains meaningful in that degenerate case by treating missing channels as unobserved.

The disturbance to be inferred is an influx boundary profile. When gas enters the annulus from the formation, it can be modeled as an unknown source term localized near $z = L$, possibly distributed over a short interval to represent perforation or open-hole length [11]. Denote the unknown free-gas mass influx rate by $\dot{m}_{in}(t)$ and, if relevant, a dissolved-gas influx component by $\dot{m}_{in,d}(t)$. The inverse problem is to estimate $\dot{m}_{in}(t)$ along with the distributed state $x(z,t)$ given $y(t)$.

A central challenge is structural non-uniqueness. Under shut-in conditions, for example, pressure diffusion-like effects, gas migration, and dissolution can produce pressure signals that resemble those from small surface choke adjustments or temperature-driven density changes. Under static conditions, machine-learning analyses have associated pressure-gradient evolution with observed annular flow patterns and achieved about 90–94% kick prognosis accuracy using neural models, suggesting that pressure-gradient carries discriminative information even when flow is not circulating [12]. The implication for physics-based estimation is that pressure-gradient information, when properly modeled, can regularize the inverse problem, but only if the forward model captures the mechanisms that shape that gradient, including compressibility, slip, and dissolution [13].

To formalize the estimation target, define the state vector

$$x(z,t) = \begin{bmatrix} p(z,t) & \alpha(z,t) & u_\ell(z,t) & u_g(z,t) & T(z,t) & x_d(z,t) \end{bmatrix}^\top. \tag{2}$$

The state evolves under a system of conservation laws with closures for slip, friction, heat transfer, and phase equilibrium. The estimator will reconstruct $x(z,t)$ over a finite horizon $[t_k - \Delta, t_k]$ and infer $\dot{m}_{in}(t)$ over the same horizon. The decision-support layer then maps the inferred state distribution into

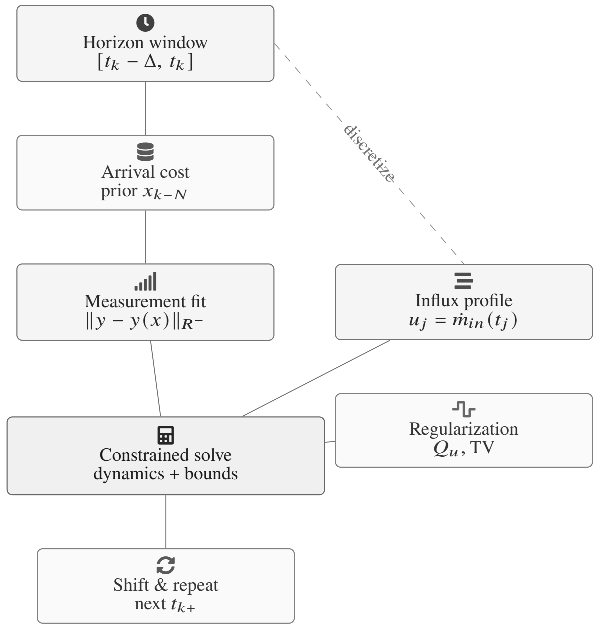

Figure 3 Moving-horizon inference loop: a sliding time window jointly estimates distributed states and an unknown influx profile by minimizing measurement mismatch with arrival-cost anchoring and smoothness regularization, subject to conservation-law dynamics and physical inequality constraints.

risk metrics and recommended responses, such as whether to initiate a controlled shut-in or adjust choke settings to maintain bottomhole pressure within safe bounds.

Observability depends on excitation and on the coupling between measured variables and latent states [14]. Even if only surface pressure is measured, a temporally rich pressure trace can carry information about downhole gas inventory because the compressible free-gas volume changes nonlinearly with pressure and temperature, and because the effective hydrostatic head depends on holdup. However, if solubility is significant, changes in dissolved fraction can buffer free-gas volume, causing two different downhole inventories to produce similar surface pressure. This motivates explicitly modeling solubility and jointly estimating dissolved and free components rather than treating the gas as purely free [15].

3. Thermo-Hydraulic Forward Model with Solubility Coupling

The forward model is one-dimensional along the annulus axis and is designed to be compatible with real-time inversion. The intent is not to resolve detailed three-dimensional flow patterns, but to capture the dominant couplings that shape pressure evolution and gas inventory.

Mass conservation is written separately for free gas, liquid, and dissolved gas within the liquid. Let $m_d = \rho_\ell(- \alpha)x_d$ denote dissolved-gas mass per unit volume of mixture. Let $\Gamma(z,t)$ denote the interphase mass transfer rate from dissolved to free gas, positive for exsolution and negative for dissolution [16]. Then

$$\frac{\partial}{\partial t}(\rho_g \alpha) + \frac{\partial}{\partial z}(\rho_g \alpha u_g) = s_g(z,t) + \Gamma(z,t), \tag{3}$$

$$\frac{\partial}{\partial t}(\rho_\ell(- \alpha)) + \frac{\partial}{\partial z}(\rho_\ell(- \alpha)u_\ell) = s_\ell(z,t), \tag{4}$$

$$\frac{\partial}{\partial t}(\rho_\ell(- \alpha)x_d) + \frac{\partial}{\partial z}(\rho_\ell(- \alpha)x_d u_\ell) = s_d(z,t) - \Gamma(z,t), \tag{5}$$

where s_g represents the influx source (localized near $z = L$), s_ℓ represents any imposed liquid injection or loss (often zero in the annulus away from boundaries), and s_d can represent a dissolved component introduced with the influx if applicable. In typical kick scenarios, s_g dominates near the entry zone and is zero elsewhere.

Momentum balance can be expressed at the mixture level to reduce stiffness while retaining slip through closure relations. Let $\rho_m = \rho_g\alpha + \rho_\ell(- \alpha)$ and define a mixture momentum flux [17]. A convenient form is

$$\frac{\partial}{\partial t}(\rho_m u_m) + \frac{\partial}{\partial z}(\rho_m u_m + p) = -\rho_m g\cos\theta(z) - \frac{f(z,t)}{D_h(z)}\rho_m u_m|u_m| + \mathcal{M}_{slip}(z,t). \tag{6}$$

where $\theta(z)$ is inclination, f is a friction factor closure that may depend on Reynolds number and effective viscosity, and $\mathcal{M}_{slip}$ accounts for the difference between phase velocities in a reduced-order manner. Alternative two-fluid momentum equations can be used, but the mixture form is advantageous for inversion

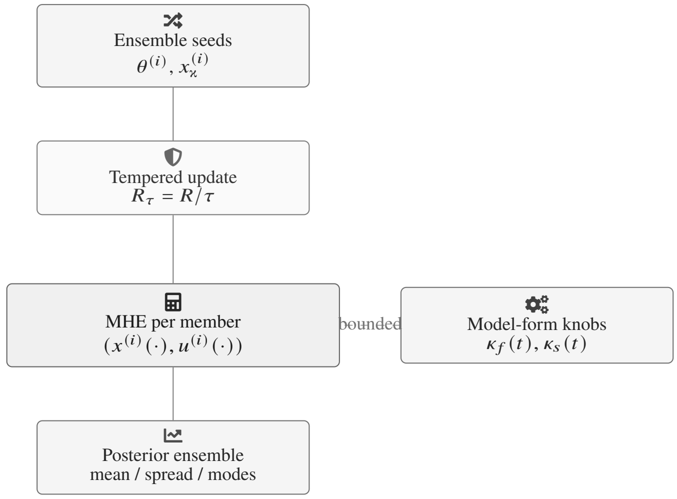

Figure 4 Robustness via ensemble inference: uncertain parameters and initial conditions generate multiple admissible reconstructions. Tempered likelihood updates mitigate overconfidence under model mismatch, while bounded correction multipliers capture systematic regime-dependent deviations without breaking conservation consistency.

because it limits the number of hyperbolic characteristics while preserving the pressure-gradient dependence on holdup.

Slip is introduced via an algebraic relation linking u_g and u_ℓ [18]. One pragmatic choice is a drift-flux-like relation

$$u_g = u_m + V_d(\alpha, p, T, \theta), \quad u_\ell = u_m - \frac{\alpha}{-\alpha} V_d(\alpha, p, T, \theta), \tag{7}$$

where V_d is a drift velocity closure capturing buoyancy-driven rise and regime-dependent slip. Because detailed regime maps are uncertain, V_d is parameterized with a small number of tunable coefficients that can be estimated or marginalized in the inference layer. This choice makes slip uncertainty explicit rather than hiding it behind a fixed regime label [19].

Energy balance is included in a reduced form to enable solubility dependence on temperature. Let $T(z,t)$ satisfy

$$\rho_m c_p \frac{\partial T}{\partial t} + \rho_m c_p u_m \frac{\partial T}{\partial z} = -h_w(z)\,(T - T_w(z)) + \Phi(z,t), \tag{8}$$

where c_p is an effective heat capacity, h_w is a wall heat transfer coefficient, $T_w(z)$ is an imposed formation or wall temperature profile, and Φ represents viscous dissipation or other small sources often neglected. The model is not intended to predict detailed thermal transients; rather, it provides a consistent temperature field that affects gas density and solubility [20].

Thermodynamics enters through the equation of state for the free gas and the phase equilibrium relation for dissolution. For the gas, a compressibility factor $Z(p,T)$ is obtained from a cubic equation of state, giving

$$\rho_g(p,T) = \frac{p M_g}{Z(p,T) R T}, \tag{9}$$

with molar mass M_g and universal gas constant R. For dissolution, define an equilibrium dissolved mass fraction $x_d^{eq}(p,T)$ that increases with pressure and decreases with temperature. A general representation is [21]

$$x_d^{eq}(p,T) = \mathcal{S}(p,T;\beta), \tag{10}$$

where $\mathcal{S}$ is a solubility function parameterized by coefficients β that reflect mud chemistry. The key is to avoid purely empirical low-pressure Henry behavior when operating at elevated pressures where non-idealities matter. A thermodynamic approach based on fugacity equality between phases provides a consistent method to compute $\mathcal{S}$, and a solubility-informed kick model has shown agreement with a chemical process simulator within a maximum deviation of 8% for methane liquid-phase mole fraction while matching bubble-point estimates, indicating that a relatively compact thermodynamic formulation can be practically accurate for this purpose [22]. In the present framework, this motivates computing x_d^{eq} from a non-ideal equilibrium relation rather than assuming negligible solubility.

Mass transfer Γ is modeled as relaxation toward equilibrium with a finite rate to represent finite kinetics and mixing limitations:

$$\Gamma(z,t) = k_m(z,t)\left(\rho_\ell(-\alpha) x_d^{eq}(p,T) - \rho_\ell(-\alpha) x_d\right), \tag{11}$$

with mass transfer coefficient k_m that may depend on shear rate, holdup, and flow rate [23]. In many operational contexts, k_m can be large relative to the transport time scale, making dissolution near-equilibrium; however, explicitly retaining kinetics prevents unphysical instantaneous transitions during sharp pressure transients and gives the estimator a degree of freedom to represent delayed exsolution.

To close the system, fluid properties $\rho_\ell(p,T)$ and $\mu_\ell(p,T)$ are parameterized, and the friction factor f is computed from an effective Reynolds number:

$$Re(z,t) = \frac{\rho_m |u_m| D_h}{\mu_{eff}(\dot{\gamma}, p, T, \alpha)}, \quad f = \mathcal{F}(Re, \epsilon/D_h), \tag{12}$$

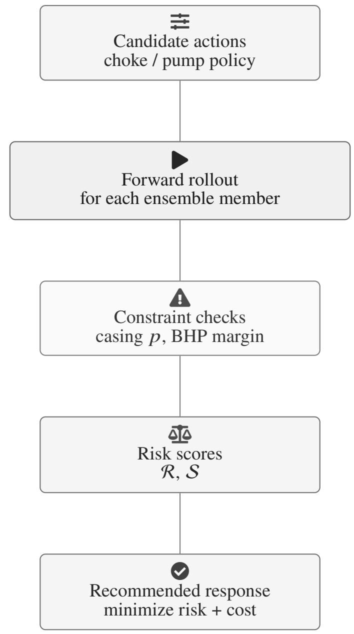

Figure 5 Risk-calibrated decision support: candidate operational responses are evaluated by forward-simulating the posterior ensemble over a lookahead horizon and computing probability/severity of constraint violation, enabling conservative choices even under non-unique downhole reconstructions.

where ϵ is roughness and μ_{eff} is an effective viscosity reflecting rheology and gas loading. The estimator treats selected property parameters as uncertain and carries them as augmented states or nuisance variables.

The boundary conditions depend on the operational mode [24]. Under circulation, an imposed liquid flow rate at $z = L$ (near the bit) and an imposed surface pressure or choke relation at $z = \varkappa$ may apply. Under shut-in, surface flow is constrained to zero and the surface pressure evolves due to compressibility and gas migration. The model supports both by switching boundary constraints while maintaining the same interior equations.

This forward model is intentionally compact: it captures compressibility, hydrostatic head changes due to holdup, frictional effects, and dissolution buffering [25]. These mechanisms are the primary determinants of how surface pressure responds to downhole gas inventory. The model is still imperfect, especially regarding regime-dependent slip and transient friction. The next sections show how the inverse formulation is designed to remain useful even when these closures are uncertain.

4. Constrained Moving-Horizon Inference of Influx and Distributed State

The inverse problem is posed as a moving-horizon estimation (MHE) problem with constraints [26]. At discrete times t_k, consider a finite horizon $[t_k - \Delta, t_k]$. The estimator seeks the state trajectory $x(z,t)$ and unknown influx profile $\dot{m}_{in}(t)$ that best explain measurements while satisfying the forward model.

Let $\mathcal{G}$ denote the discretized forward operator mapping initial state and inputs to predicted measurements. Denote the discretized state at time index j by x_j and the influx control at the same index by $u_j = \dot{m}_{in}(t_j)$. The total-variation term promotes piecewise-smooth influx behavior, consistent with a kick onset followed by a plateau or decay, without requiring explicit change-point detection.

The optimization is subject to equality constraints given by the discretized conservation laws: [27]

$$x_{j+} = \mathcal{F}(x_j, u_j, \theta_j), \quad j = k - N, \dots, k - , \tag{13}$$

where θ_j denotes nuisance parameters such as slip coefficients or friction multipliers, which may be held fixed, estimated, or marginalized. Inequality constraints enforce physical admissibility:

$$\varkappa \le \alpha_j \le , \quad \varkappa \le x_{d,j} \le x_{d,\max}, \quad p_j \ge p_{min}, \quad u_j \ge \varkappa, \tag{14}$$

where bounds reflect plausible ranges and prevent the optimizer from exploiting nonphysical states to match noisy measurements.

A key difficulty is that the mapping from influx to surface pressure is often weakly identifiable for short horizons, particularly if gas dissolves significantly [28]. To improve identifiability, the estimator uses the full state coupling: pressure evolution depends on both free-gas compressibility and hydrostatic changes, while dissolution affects the partitioning and thus changes the effective compressibility of the mixture. Even if surface pressure alone is used, the time derivative and curvature of the pressure trace over the horizon provide information about the evolving mixture compressibility and holdup distribution. The MHE formulation naturally exploits this by matching the entire time series rather than a single snapshot.

Because the forward model is nonlinear and stiff, gradient-based optimization benefits from adjoint sensitivities [29]. For a discretized system, the adjoint recursion can be written schemat-

Table 1 Dominant physical mechanisms shaping surface responses during multiphase kicks.

Mechanism	Effect on surface response	Representation in framework
Gas compressibility	Nonlinear pressure–volume relation; strong curvature in shut-in pressure traces	Real-gas EOS with compressibility factor $Z(p, T)$ for free gas density ρ_g
Holdup evolution	Changes effective hydrostatic head and mixture density along the annulus	One-dimensional transport of void fraction $\alpha(z, t)$ coupled to mixture momentum
Gas dissolution	Buffers free-gas volume and delays pressure response to influx	Dissolved-gas state $x_d(z, t)$ with pressure- and temperature-dependent equilibrium $x_d^{eq}(p, T)$
Slip between phases	Modifies gas rise rate and pressure-gradient structure, affecting timing of surface signatures	Drift-flux-type slip closure via drift velocity $V_d(\alpha, p, T, \theta)$
Friction and heat transfer	Alters pressure gradient under circulation and influences temperature-dependent properties	Friction factor $f(Re)$ and wall heat transfer $h_w(z)$ in momentum and energy balances

ically as

$$\lambda_j = \left(\frac{\partial \mathcal{F}}{\partial x_j}\right)^{\top} \lambda_{j+} + \left(\frac{\partial y_j}{\partial x_j}\right)^{\top} R^{-} \left(y_j - y_j(x_j)\right), \qquad (15)$$

with terminal condition derived from the final measurement mismatch and, if applicable, terminal penalties. The gradient with respect to influx is then

$$\frac{\partial J}{\partial u_j} = -\left(\frac{\partial \mathcal{F}}{\partial u_j}\right)^{\top} \lambda_{j+} + Q_u^{-} u_j + \lambda_{TV}\, \partial |u_{j+} - u_j|, \qquad (16)$$

where the last term is interpreted in a subgradient sense [30]. In practice, a smooth approximation to absolute value can be used to facilitate stable convergence.

Spatial discretization must preserve mass conservation and handle advection-dominated transport. A finite-volume method with approximate Riemann solvers or flux limiters is suitable [31]. For inversion, numerical diffusion can be beneficial in moderation because it regularizes sharp fronts that the sparse measurement set cannot resolve. However, excessive diffusion can smear gas fronts and bias estimated influx duration. The chosen discretization therefore balances stability, conservation, and identifiability.

The arrival cost P is updated recursively, either via a local linearization or via an ensemble approximation [32]. This allows the estimator to summarize the influence of past data without extending the horizon indefinitely. When computational budget is limited, the estimator can reduce the decision variables by representing $u(t)$ over the horizon using a low-dimensional basis, such as a small set of spline coefficients, while still enforcing the conservation-law constraints. This basis compression is particularly useful when only surface pressure is measured, because it prevents overfitting with high-frequency influx oscillations that cannot be supported by the data.

The inference scheme also supports mode switching [33]. Under circulating conditions, the boundary condition at $z = L$ typically imposes liquid flow, while under shut-in, flow is constrained and the system becomes more sensitive to gas migration and dissolution. The MHE problem changes its boundary constraints accordingly, but the interior dynamics remain the same. This yields a unified estimator across operational modes, which is important because transitions between circulation and shut-in are themselves informative events that the estimator must interpret without losing continuity [34].

5. Uncertainty Propagation, Model-Form Robustness, and Risk Metrics

Even with careful constraints, the inverse problem remains uncertain. Slip closures, friction factors, and heat transfer coefficients can vary with flow regime and cuttings loading, and the measurement model can be contaminated by surface equipment dynamics. Treating the MHE solution as a single deterministic estimate can be misleading if multiple distinct downhole states produce similar surface signals. The framework therefore couples MHE with uncertainty propagation to produce a posterior distribution over states and influx [35].

A practical approach is an ensemble MHE, where a set of particles or ensemble members represent uncertain parameters and initial states. Each member solves an MHE problem with perturbed parameters and noise realizations, producing an ensemble of admissible trajectories. Let $\{x^{(i)}(z, t), u^{(i)}(t)\}_{i=}^{M}$ denote the ensemble. The empirical mean and covariance provide a local uncertainty quantification, while the diversity of inferred influx profiles indicates identifiability.

To avoid degeneracy where all ensemble members collapse to a narrow region due to overconfident arrival costs, the estimator uses inflation or tempering strategies [36]. For example, the

Table 2 Distributed thermo-hydraulic state variables in the annular model.

Symbol	Description	Units	Primary role
$p(z,t)$	Pressure along the annulus	Pa	Governs gas density, solubility, and hydrostatic head
$\alpha(z,t)$	Free-gas volumetric fraction (void fraction)	–	Sets mixture density and compressibility
$u_\ell(z,t)$	Liquid superficial velocity	m/s	Contributes to mass transport and momentum balance
$u_g(z,t)$	Gas superficial velocity	m/s	Captures gas migration and slip relative to liquid
$T(z,t)$	Mixture temperature	K	Affects fluid properties and $x_d^{eq}(p,T)$
$x_d(z,t)$	Dissolved-gas mass fraction in liquid	–	Tracks gas stored in liquid phase and exsolution potential

Table 3 Representative measurement configurations at the surface.

Scenario	Available channels $y(t)$	Comments for estimation
Pressure-only	Wellhead pressure $p(\varkappa,t)$	Minimal configuration; still informative via temporal curvature
Pressure + flow	$p(\varkappa,t)$ and bulk flow rate $q_m(\varkappa,t)$	Improves identifiability of friction and holdup
Pressure + phase flow	$p(\varkappa,t)$, $q_\ell(\varkappa,t)$, $q_g(\varkappa,t)$	Enables separate constraints on gas and liquid inventories
Pressure + density log	$p(\varkappa,t)$ and inferred outlet density	Provides direct information on mixture compressibility
Multi-mode logging	Combination of high-rate pressure with slower pit and flow data	Handled by treating missing or delayed channels as unobserved

measurement likelihood can be raised to a power $\tau \in (\varkappa,]$ to soften updates when the model mismatch is suspected, effectively enlarging R:

$$R_\tau = \frac{}{\tau} R. \tag{17}$$

This prevents the inversion from forcing the state into implausible regions to exactly match measurements that include unmodeled choke dynamics.

Model-form robustness is addressed by augmenting the state with low-dimensional correction terms that can absorb systematic bias without violating conservation. One approach is to introduce a friction multiplier $\kappa_f(t)$ and a slip multiplier $\kappa_s(t)$ that scale nominal closures: [37]

$$f \leftarrow \kappa_f(t) f_\varkappa(Re, \epsilon/D_h), \quad V_d \leftarrow \kappa_s(t) V_{d,\varkappa}(\alpha, p, T, \theta). \tag{18}$$

These multipliers are constrained to remain within plausible ranges and are penalized for rapid variation. This allows the estimator to accommodate regime-induced changes in friction and slip without explicitly classifying regimes. Importantly, the multipliers remain interpretable as effective corrections rather than opaque latent variables [38].

Decision support is framed through risk metrics derived from the posterior ensemble. Let $C(x)$ denote a constraint function representing an operational limit, such as maximum allowable casing pressure at surface or minimum bottomhole pressure relative to pore pressure. Define a risk probability over a lookahead horizon H:

$$\mathcal{R}(t_k) = \mathbb{P}\left(\max_{t \in [t_k, t_k+H]} C(x(t)) > \varkappa \,\middle|\, y_{\varkappa:k} \right). \tag{19}$$

This probability is approximated by the ensemble fraction violating the constraint under forward simulation using candidate

Table 4 Summary of governing conservation equations in the forward model.

Equation	Conserved quantity	Dominant modeled effects	Notes
Gas mass balance	Free-gas mass $\rho_g \alpha$	Influx source s_g, compressibility, slip transport, exsolution term Γ	Localized influx near $z = L$
Liquid mass balance	Liquid mass $\rho_\ell(- \alpha)$	Injection or loss s_ℓ, hydrostatic and friction coupling	Often no interior source term
Dissolved-gas balance	Dissolved mass $\rho_\ell(- \alpha) x_d$	Influx s_d and mass transfer Γ	Allows delayed exsolution after influx
Mixture momentum	Mixture momentum $\rho_m u_m$	Gravity, friction, interphase slip, pressure gradient	Reduced-order closure for slip effects
Energy balance	Thermal energy	Convective transport, wall heat exchange, property variation	Supports temperature-dependent solubility

Table 5 Solubility and mass-transfer quantities for gas in non-aqueous drilling fluids.

Quantity	Definition	Role in kick dynamics
$x_d(z,t)$	Dissolved-gas mass fraction in the liquid phase	Measures gas buffered in the liquid
$x_d^{eq}(p,T)$	Equilibrium dissolved fraction from solubility function $\mathcal{S}(p,T;\beta)$	Sets target for dissolution/exsolution at given p, T
$\Gamma(z,t)$	Interphase mass-transfer rate between dissolved and free gas	Controls rate of approach to equilibrium
$k_m(z,t)$	Effective mass-transfer coefficient	Encodes mixing and kinetic limitations
Solubility parameters β	Coefficients in non-ideal thermodynamic model	Capture mud chemistry and pressure dependence of x_d^{eq}

control actions. The estimator thus supports not only diagnosis (what is happening) but prognosis (what will happen under different responses) [39].

A complementary metric is the expected severity, which weights violations by magnitude:

$$\mathcal{S}(t_k) = \mathbb{E}\left[\int_{t_k}^{t_k+H} \max(\varkappa, C(x(t)))\, dt \,\middle|\, y_{\varkappa:k}\right]. \tag{20}$$

These metrics allow ranking candidate actions without claiming certainty. For example, a choke adjustment policy can be evaluated by simulating each ensemble member forward, applying the policy, and computing $\mathcal{R}$ and $\mathcal{S}$. The recommended action is then one that minimizes a weighted combination of risk and operational cost while respecting constraints:

$$\pi^\star = \arg\min_{\pi\in\Pi} \quad w_R \mathcal{R}_\pi(t_k) + w_S \mathcal{S}_\pi(t_k) + w_U \mathbb{E}\left[\int_{t_k}^{t_k+H} \ell(u_c(t))\, dt\right], \tag{21}$$

where π denotes a control policy mapping measurements to choke commands $u_c(t)$, ℓ is an actuation cost, and w_R, w_S, w_U are weights reflecting operational preferences [40].

Because this paper focuses on estimation, the control policy class Π is kept simple, such as affine feedback on surface pressure deviation with saturation. The key point is that the risk evaluation is grounded in the physically constrained posterior ensemble, not in a single point estimate. This reduces the chance of brittle decisions when the inverse problem is ill-conditioned.

Table 6 Components of the moving-horizon estimation objective.

Term	Mathematical form	Physical interpretation	Tuning handle
Measurement fit	$\sum \lVert y_j - y_j(x_j) \rVert_{R^-}$	Penalizes misfit between predicted and measured surface data	Measurement covariance R
Arrival cost	$\lVert x_{k-N} - \hat{x}_{k-N} \rVert_{P^-}$	Encodes prior state information from earlier horizon	Arrival covariance P
Influx magnitude	$\sum \lVert u_j \rVert_{Q_u^-}$	Discourages unrealistically large influx rates	Weighting matrix Q_u
Influx smoothness	$\lambda_{TV} \sum \lvert u_{j+} - u_j \rvert$	Promotes piecewise-smooth influx with few sharp jumps	Total-variation weight λ_{TV}
Parameter variation	Optional penalties on slip or friction multipliers	Limits rapid changes in effective closures	Multiplier regularization weights

Table 7 Physical and operational constraints enforced in the estimator.

Constraint	Mathematical form	Purpose
Void fraction bounds	$\varkappa \leq \alpha(z,t) \leq$	Prevents nonphysical gas fractions and negative liquid content
Dissolved fraction bounds	$\varkappa \leq x_d(z,t) \leq x_{d,\max}$	Limits dissolved inventory to thermodynamically plausible range
Pressure limits	$p(z,t) \geq p_{\min}$ and casing limits at surface	Enforces safety margins relative to collapse and equipment ratings
Influx non-negativity	$u_j = \dot{m}_{in}(t_j) \geq \varkappa$	Avoids artificial outflow from formation in the inverse solution
Closure multipliers	$\kappa_f^{\min} \leq \kappa_f(t) \leq \kappa_f^{\max}$, similarly for κ_s	Constrains effective friction and slip corrections
Mode-dependent boundaries	Circulation vs shut-in boundary conditions	Ensures consistency with operational mode transitions

6. Physics-Constrained Surrogates as Optional Accelerators

Real-time estimation can be computationally demanding if each MHE iteration requires repeated forward simulations of a nonlinear PDE system [41]. To reduce cost without sacrificing physical plausibility, the framework allows a physics-constrained surrogate to accelerate the forward operator or its sensitivities. The surrogate is not the primary model; it is a helper that approximates parts of the computation while the mechanistic constraints remain enforced either exactly or through residual penalties.

One strategy is to learn a surrogate mapping from a compressed representation of the state and influx to surface measurements over short horizons [42]. Let $r(t)$ denote a reduced representation of the downhole state, such as a small set of moments of holdup and dissolved-gas inventory:

$$r(t) = \left[\int_{\varkappa}^{L} \alpha(z,t)\, dz \quad \int_{\varkappa}^{L} \rho_\ell(-\alpha) x_d\, dz \quad \int_{\varkappa}^{L} p(z,t)\, dz \quad p(L,t) \right]^\top . \tag{22}$$

A surrogate $\mathcal{H}$ approximates the mapping to surface pressure increment:

$$p(\varkappa, t+\delta) - p(\varkappa, t) \approx \mathcal{H}\left(r(t), u(t:t+\delta) \right) . \tag{23}$$

Training data can be generated from the mechanistic model under randomized parameters. The surrogate then serves as a cheap predictor inside a proposal step or within a coarse-to-fine optimization loop, where candidate influx profiles are screened quickly before being refined with the full PDE model.

To avoid the surrogate drifting into nonphysical regions, training includes a physics residual penalty computed from the

Table 8 Examples of uncertain parameters treated within the estimation framework.

Parameter	Physical meaning	Uncertainty source	Treatment
Slip coefficients	Parameters in drift velocity $V_d(\cdot)$	Regime-dependent gas–liquid interaction	Augmented state or ensemble dispersion
Friction factor multiplier κ_f	Effective scaling of nominal friction closure	Cuttings loading, roughness, flow regime	Estimated with bounds and regularization
Solubility parameters β	Governing $x_d^{eq}(p, T)$	Mud formulation, lab-to-field mismatch	Calibrated and perturbed in ensembles
Mass-transfer coefficient k_m	Rate of dissolution/exsolution	Unknown mixing and kinetic effects	Treated as uncertain but slowly varying
Wall heat transfer $h_w(z)$	Coupling to formation temperature	Thermal model simplifications	Represented via uncertain profile or scalar factor

Table 9 Synthetic scenario families used in computational experiments.

Scenario family	Primary variation	Purpose	Typical mode
Solubility sweep	Scaling of $\mathcal{S}(p, T)$ from negligible to strong dissolution	Assess impact of dissolution on inferred influx	Circulation and shut-in
Slip uncertainty	Drift-velocity coefficients modified for slow/fast gas rise	Test ambiguity between holdup distribution and mass	Mostly shut-in
Friction perturbation	Time-varying $\kappa_f(t)$ mimicking cuttings or regime shifts	Examine misinterpretation of friction changes as influx	Circulating segments
Boundary mode switch	Transitions between circulating and shut-in constraints	Use mode changes as excitation for identifiability	Mixed operation
Noise and filtering	Different sensor noise levels and low-pass filters	Evaluate robustness to surface measurement quality	All scenarios

mechanistic equations projected onto the reduced coordinates [43]. For instance, if $\mathcal{E}(x, u) = \varkappa$ denotes the discretized conservation residual, the loss can include

$$\mathcal{L} = \sum_n \left\| p_\varkappa^{(n)} - p_\varkappa^{(n)} \right\| + \lambda_E \sum_n \left\| \mathcal{E}\left(x^{(n)}, u^{(n)}\right) \right\|, \qquad (24)$$

where $x^{(n)}$ is the surrogate-implied state reconstruction. Even if the surrogate is only approximate, the residual term encourages consistency with conservation and reduces catastrophic extrapolation.

A second strategy is to surrogate only specific closures, such as friction factor multipliers or slip drift velocity, conditioned on local state variables. This reduces model-form error while keeping the conservation-law skeleton intact. For example, a small neural closure can map (Re, α, θ) to κ_f with smoothness constraints [44]. In inversion, this closure can be treated as a parameterized function whose parameters are updated slowly, while the main state is estimated via MHE. This is a pragmatic compromise: regime effects are captured adaptively, but the estimator remains constrained by the mechanistic transport equations.

Importantly, none of these accelerators require flow-pattern labels. They learn directly from simulated or historical data in terms of measurable quantities like pressure and flow, and they are used only to speed computation or reduce systematic bias [45]. The final inferred state must still satisfy the mechanistic constraints to the degree enforced by the estimator, ensuring that interpretability and conservation are not traded away for speed.

7. Computational Experiments and Discussion

This section reports numerical experiments designed to stress the estimator under realistic ambiguities. The goal is not to claim universal performance, but to demonstrate how the proposed coupling of solubility-aware physics and constrained inversion changes the qualitative identifiability of influx size and distribution relative to solubility-ignorant or unconstrained

Table 10 Risk-oriented decision metrics derived from posterior ensembles.

Metric	Definition (conceptual)	Operational interpretation
Constraint-violation probability $\mathcal{R}(t_k)$	Fraction of ensemble trajectories that violate a pressure or holdup limit within lookahead horizon H	Probability that a candidate choke action leads to unsafe conditions
Expected severity $\mathcal{S}(t_k)$	Ensemble-averaged time integral of constraint violation magnitude	Expected extent or duration of limit exceedance
Gas-at-shoe exceedance	Probability that gas holdup at casing shoe exceeds a threshold	Quantifies risk of gas reaching critical depths
Pit-gain forecast	Distribution of future pit gain under candidate actions	Links inferred influx and dissolution dynamics to volume-based alarms
Action ranking score	Weighted combination of risk, severity, and actuation cost	Supports selection among candidate choke policies

alternatives [46].

The computational domain represents an annulus of length L with variable inclination and modest geometric variation. Boundary conditions are chosen to emulate two modes: circulating and shut-in. In circulating mode, a constant liquid flow is imposed at the lower boundary, and surface pressure is allowed to evolve under a choke relation with finite response time. In shut-in mode, surface flow is constrained to zero and surface pressure evolves due to compressibility and migration [47]. Gas influx is injected near the lower boundary using a smooth onset profile, then turned off, so that both onset detection and post-influx migration are present.

Three scenario families are considered. The first family varies solubility strength by scaling $\mathcal{S}(p,T)$, producing cases with negligible dissolution, moderate dissolution, and strong dissolution. The second family varies slip uncertainty by modifying drift velocity coefficients, producing faster or slower gas rise. The third family introduces friction perturbations to emulate cuttings loading or regime-dependent turbulence changes, implemented as time-varying multipliers $\kappa_f(t)$ [48].

In each scenario, synthetic measurements are generated from the forward model with added noise and low-pass filtering to emulate sensor dynamics. The estimator then runs with imperfect prior parameters, including biased friction and slip coefficients, and attempts to infer influx and state. Performance is evaluated by comparing inferred influx mass, inferred gas inventory distribution, and predicted future surface pressure under a fixed test action [49].

A consistent observation across scenarios is that modeling dissolution materially changes the inferred explanation for the same surface pressure trace. In low-solubility cases, surface pressure increase and pit gain correlate strongly with free-gas expansion, and the estimator attributes observed pressure curvature primarily to gas holdup. In high-solubility cases, early-time pressure changes can be smaller because injected gas dissolves under high pressure, delaying free-gas volume growth. When the well transitions to lower pressures during migration, exsolution releases gas and produces a delayed amplification in pressure response [50]. If dissolution is ignored, the estimator tends to infer a smaller initial influx followed by an artificially prolonged influx duration to fit the delayed amplification. When dissolution is included, the estimator instead infers a more realistic short influx with subsequent exsolution-driven growth. This distinction matters operationally: a prolonged inferred influx suggests ongoing formation flow, while an exsolution-driven delay suggests that the influx has already ceased but is being revealed by thermodynamics.

Slip uncertainty produces a different ambiguity [51]. Faster slip moves gas upward more quickly, shifting the timing of surface pressure changes and reducing downhole holdup at depth. Slower slip retains gas deeper, increasing hydrostatic effects and potentially producing similar surface pressure via a different distribution. The ensemble approach captures this by producing multimodal posterior distributions in some cases, with one mode corresponding to fast-rise small influx and another to slow-rise larger influx. Deterministic inversion tends to pick one mode depending on initialization, which can lead to overconfident conclusions [52]. By contrast, the ensemble risk metrics remain meaningful: if both modes predict a high probability of exceeding a surface pressure limit under a candidate choke action, the recommended action remains conservative even when the inferred influx size differs.

Friction perturbations primarily affect the mapping between flow rate and pressure gradient, especially in circulating mode. If friction increases unexpectedly, surface pressure rises even without additional gas [53]. An unconstrained estimator may misattribute this to gas influx, leading to false positives. The augmented-state approach with $\kappa_f(t)$ reduces this failure mode by allowing the estimator to explain part of the pressure rise as frictional rather than compressibility-driven. However, the estimator does not simply absorb everything into $\kappa_f(t)$ because the conservation-law coupling imposes different temporal signatures: friction changes affect pressure drop approximately proportional to $u_m|u_m|$, while gas influx affects mixture density, compressibility, and thus the time evolution of pressure under shut-in. When both circulating and shut-in segments are present, the estimator can use the mode switch as an excitation event to distinguish these effects [54].

A central practical question is latency: how quickly can the estimator provide a stable inference after influx onset? In simulations where the influx produces a clear surface pressure deviation, the MHE typically stabilizes within a small fraction of the migration time scale, because the temporal structure of the pressure trace provides enough information to pin down the influx onset time and approximate magnitude. In more ambiguous cases, particularly under strong dissolution and slow slip, the estimator remains uncertain longer, but the risk metrics still become informative early. For example, even if the total influx mass remains uncertain, the probability of exceeding a pressure limit under an aggressive choke closure can become high across the ensemble, signaling that conservative control is warranted. This illustrates the advantage of risk-based decision support: it can be actionable before the inverse problem is fully resolved [55].

Another practical issue is sensitivity to discretization and horizon length. Short horizons reduce computation but can fail to capture delayed exsolution effects, leading to biased influx estimates. Longer horizons improve identifiability but increase cost. A hybrid strategy works well: use a short horizon for rapid onset detection and a longer horizon periodically for recalibration of dissolved inventory and solubility-related parameters [56]. Because the arrival cost summarizes past information, the longer-horizon recalibration can be done intermittently without losing continuity.

Finally, the experiments highlight that the estimator is not a flow-regime classifier, yet it can still produce regime-relevant information indirectly. Changes in inferred slip multipliers, friction multipliers, and holdup distributions correlate with regime transitions in the sense that they reflect a shift in effective transport behavior [57]. This is operationally useful because it provides quantitative parameters for forecasting rather than categorical labels. When desired, a separate classifier could be attached downstream, using the inferred state as input, but the estimator itself remains focused on conservation-consistent reconstruction.

8. Conclusion

This paper developed a physics-constrained estimation and decision-support framework for gas-kick transients using sparse surface measurements. The central premise is that surface pressure is informative but ambiguous, and that the ambiguity can only be reduced reliably by embedding measurements within a conservation-law model that accounts for compressibility, holdup evolution, and dissolution-driven buffering [58]. To that end, the work introduced a compact thermo-hydraulic forward model with explicit dissolved-gas dynamics and a solubility relation consistent with non-ideal thermodynamics, coupled to a constrained moving-horizon estimator that jointly reconstructs distributed states and an unknown influx profile. The estimator enforces physical bounds and uses regularization to prevent implausible influx oscillations, while an ensemble extension propagates parameter and model-form uncertainties to yield posterior risk metrics suitable for operational decision-making.

Computational experiments demonstrated how solubility can change the inferred interpretation of similar surface pressure traces, particularly when exsolution delays free-gas expansion and thus shifts the timing of surface responses. The experiments also illustrated how slip and friction uncertainties can create multimodal inverse solutions, and how ensemble-based risk measures can remain actionable even when influx magnitude is not uniquely identifiable [59]. Optional physics-constrained surrogates were described as accelerators that can reduce computational burden without replacing mechanistic plausibility.

The resulting framework is intended as an extensible backbone rather than a finalized product. Its value lies in providing interpretable, constraint-consistent state reconstructions with uncertainty and in enabling risk-calibrated evaluation of candidate responses. Future work can incorporate richer rheology, cuttings transport, more detailed choke and surface equipment models, and systematic calibration against field data, while retaining the same core principle: decisions should be driven by physically admissible posterior ensembles rather than by unconstrained fits to surface signals [60].

Acknowledgments

We would like to thank the reviewers of this research for their helpful comments and suggestions.

References

[1] C. Carson, "Suggested drilling research tasks for the federal government," 4 1984.

[2] A. P. Gilkey, C. W. Hansen, J. F. Schatz, D. K. Rudeen, and D. L. Lord, "Drspall :spallings model for the waste isolation pilot plant 2004 recertification.," 2 2006.

[3] C. E. Obi, Y. Falola, K. Manikonda, A. R. Hasan, and M. A. Rahman, "Flow pattern, pressure gradient relationship of gas kick under dynamic conditions," in *Offshore Technology Conference*, p. D041S053R006, OTC, 2022.

[4] T. Ponomarenko, E. Marin, and S. Galevskiy, "Economic evaluation of oil and gas projects: Justification of engineering solutions in the implementation of field development projects," *Energies*, vol. 15, pp. 3103–3103, 4 2022.

[5] C. K. Knutson and C. R. Boardman, "Assessment of non-destructive testing of well casing,, cement and cement bond in high temperature wells," 1 1979.

[6] D. Ojedeji, "Gas evolution phenomenon of methane in base fluids of non-aqueous drilling muds under controlled depressurization," 6 2021.

[7] W. J. McDonald and G. T. Pittard, "Development of a near-bit mwd system," 5 1995.

[8] "Final report on uncertainties in the detection, measurement, and analysis of selected features pertinent to deep geologic repositories," 7 1978.

[9] A. H. Salloom, O. A. Abdulrazzaq, S. Sadoon, and W. G. Abdulnaby, "A review of the geothermal potential hot spots in iraq using geophysics methods," *Journal of Petroleum Research and Studies*, vol. 12, pp. 51–69, 3 2022.

[10] M. E. Loginova and F. A. Agzamov, "Viscoelastic systems for well construction," *Kazakhstan journal for oil & gas industry*, vol. 4, pp. 58–68, 5 2022.

[11] A. Wspanialy and M. Kyaw, "Surface drilling parameters and drilling optimization techniques: Are they useful tools in gas hydrate detection?," *Energies*, vol. 15, pp. 4635–4635, 6 2022.

[12] C. E. Obi, Y. Falola, K. Manikonda, A. R. Hasan, and M. A. Rahman, "A machine learning analysis to relate flow pattern and pressure gradient during gas kicks under static conditions," in *SPE Western Regional Meeting*, p. D011S006R002, SPE, 2022.

[13] D. Cohen, J. Dallas, F. Knight, and E. Woerheide, "Development of a gas handling hydraulic submersible pump and planning a field trial, captain field," in *Offshore Technology Conference*, OTC, 5 1997.

[14] "Two-phase reaction turbine. technical progress report for the period july-december 1999," 12 1999.

[15] T. P. Beaton, R. Seale, and J. Beaird, "Development of a geared turbodrilling system and identifying applications," in *Canadian International Petroleum Conference*, PETSOC, 6 2004.

[16] "Geothermal energy in the western united states and hawaii: Resources and projected electricity generation supplies. [contains glossary and address list of geothermal project developers and owners]," 9 1991.

[17] A. K. R. Widodo, D. Rahmadona, and H. Gunawan, "Reduce-reuse-recycle approach in managing onshore drilling waste in north senoro drilling gas field development project," in *SPE/IATMI Asia Pacific Oil & Gas Conference and Exhibition*, SPE, 10 2015.

[18] R. Xu, J. Deng, and X. Liu, "Separation system design and equipments performance optimization for high-viscosity and high-density drilling fluid," in *Volume 7: Fluid Flow, Heat Transfer and Thermal Systems, Parts A and B*, pp. 1177–1180, ASMEDC, 1 2010.

[19] M. P. Starrett, A. D. Hill, and K. Sepehrnoori, "A shallow-gas-kick simulator including diverter performance," *SPE Drilling Engineering*, vol. 5, pp. 79–85, 3 1990.

[20] A. T. Bozdana and N. K. Al-Karkhi, "Comparative experimental investigation and gap flow simulation in electrical discharge drilling using new electrode geometry," *Mechanical Sciences*, vol. 8, pp. 289–298, 9 2017.

[21] T. Mokhalalati, A. Al-Suwaidi, and A. E.-F. Hendi, "Managing onshore drilling wastes - abu dhabi experience," in *Abu Dhabi International Petroleum Exhibition and Conference*, SPE, 10 2000.

[22] K. Manikonda, A. R. Hasan, N. H. Rahmani, O. Kaldirim, C. E. Obi, J. J. Schubert, and M. A. Rahman, "A gas kick model that uses the thermodynamic approach to account for gas solubility in synthetic-based mud," in *SPE/IADC Middle East drilling Technology conference and exhibition*, p. D031S016R001, SPE, 2021.

[23] "Development and testing of a high-pressure downhole pump for jet-assist drilling. final report," 7 1996.

[24] M. Reich, M. Oesterberg, H. Montes, and J. Treviranus, "Straight down to success: Performance review of a vertical drilling system," in *SPE Annual Technical Conference and Exhibition*, SPE, 10 2003.

[25] C. Harvey, "Sperry low temperature geothermal conversion system, phase i and phase ii. volume iv. field activities. final report," 1 1984.

[26] Y. Wang, G. Wen, and H. Chen, "Horizontal directional drilling-length detection technology while drilling based on bi-electro-magnetic sensing.," *Sensors (Basel, Switzerland)*, vol. 17, pp. 967–, 4 2017.

[27] "Development of a natural gas systems analysis model (gsam). annual report," 2 1994.

[28] W. Maurer, W. Deskins, W. McDonald, J. Cohen, F. Heuze, and M. Butler, "Rapid deployment drilling system for onsite inspections under a comprehensive test ban preliminary engineering design," 9 1996.

[29] R. Thomas, R. Chapman, and H. Dykstra, "Reservoir assessment of the geysers geothermal field," 1 1981.

[30] D. Wootan, R. Bolden, A. Bridges, N. Cannon, S. Chastain, B. Hey, R. Knight, C. Linschooten, A. Pitner, and B. Webb, "Summary report on the design of the retained gas sampler system (retained gas sampler, extruder and extractor)," 9 1994.

[31] A. Alfakih, A. Galaby, N. Sadiq, R. Famiev, and M. K. Nafi, "Drilling and cementing through highly active shallow gas field," in *ADIPEC*, SPE, 10 2022.

[32] A. A. Almashwali, B. Lal, A. S. Maulud, and K. S. Foo, "Kinetic inhibition effect of valine on methane hydrate nucleation time in oil system," *Key Engineering Materials*, vol. 938, pp. 133–138, 12 2022.

[33] K. Dollens, K. Harpole, E. Durrett, and J. Bles, "Design and implementation of a cosub 2 flood utilizing advanced reservoir characterization and horizontal injection wells in a shallow shelf carbonate approaching waterflood depletion. annual report, july 1, 1996–june 30, 1997," 12 1997.

[34] A. Al-Momin, M. Kurdi, S. Baki, K. Mechkak, and A. Al-Saihati, "Proving the concept of unconventional gas reservoirs in saudi arabia through multistage fractured horizontal wells," in *SPE Asia Pacific Unconventional Resources Conference and Exhibition*, SPE, 11 2015.

[35] K. D. Lyons, S. Honeygan, and T. Mroz, "Netl extreme drilling laboratory studies high pressure high temperature drilling phenomena," in *Volume 2: Structures, Safety and Reliability; Petroleum Technology Symposium*, pp. 791–796, ASMEDC, 1 2007.

[36] M. Matsuzawa, Y. Terao, B. Hay, L. Wingstrom, M. Duncan, and I. Ayling, "A completion system application for the world's first marine hydrate production test," in *Offshore Technology Conference*, OTC, 5 2014.

[37] R. W. Ahmad, K. Salah, R. Jayaraman, I. Yaqoob, and M. Omar, "Blockchain in oil and gas industry: Applications, challenges, and future trends," 10 2021.

[38] F. Andritsos and H. Cozijn, "An innovative oil pollution containment method for ship wrecks proposed for offshore well blow-outs," in *Volume 2: Structures, Safety and Reliability*, pp. 73–81, ASMEDC, 1 2011.

[39] M. H. Mahmoud, "Underwater precast reinforced concrete silo for oil drilling and production applications," in *Offshore Technology Conference*, OTC, 5 2017.

[40] C. Dong, Y. Li, Q. Zhang, S. Feng, and L. Zhang, "Experimental study on sand-carrying mechanism and capacity evaluation in water-producing gas wells and its application in artificial lift optimization," in *SPE Middle East Artificial Lift Conference and Exhibition*, SPE, 11 2014.

[41] F. Fleyfel, C. Silva, G. Okoh, O. Ilesanmi, A. Rivas-Cardona, E. Marotta, and J. Fayemi, "Multiphase cfd cool-down behaviors of an evdt and manifold systems," in *Offshore Technology Conference*, OTC, 5 2013.

[42] M. Kang, S. Christian, M. A. Celia, D. L. Mauzerall, M. Bill, A. R. Miller, Y. Chen, M. E. Conrad, T. H. Darrah, and R. B. Jackson, "Identification and characterization of high methane-emitting abandoned oil and gas wells," *Proceedings of the National Academy of Sciences of the United States of America*, vol. 113, pp. 13636–13641, 11 2016.

[43] Q. Nie, S. Zhang, Y. Huang, X. Yi, and J. Wu, "Numerical and experimental investigation on safety of downhole solid–liquid separator for natural gas hydrate exploitation," *Energies*, vol. 15, pp. 5649–5649, 8 2022.

[44] R. Boger, "Report on testing to expand the rotary mode core sampling operating envelope," 12 1999.

[45] N. G. Author, "Testing geopressured geothermal reservoirs in existing wells. saldana well no. 2, zapata county, texas. volume i. completion and testing. final report," 10 1981.

[46] S. Wolhart, "Stimulation technologies for deep well completions," 6 2003.

[47] C.-H. Yang, P.-P. Lu, Y.-M. Cao, M. Xu, Z.-Y. Yu, and P.-F. Cheng, "Study on the plugging limit and combination of co2 displacement flow control system based on nuclear magnetic resonance (nmr)," *Processes*, vol. 10, pp. 1342–1342, 7 2022.

[48] "Rawlins ucg demonstration project. final technical progress report, january 1, 1987–february 9, 1988," 8 1988.

[49] J. Wang, J. Sun, X. Xue, Y. Qu, R. Bai, B. Zhang, and Y. Wang, "Development of hydraulic flow control valve for intelligent gas well," in *Proceedings of the 2022 2nd International Conference on Control and Intelligent Robotics*, pp. 468–478, ACM, 6 2022.

[50] S. Varnado, "Geothermal drilling and completion technology development program. annual progress report, october 1979-september 1980," 11 1980.

[51] C. Johnson, C. Augustine, and M. Goldberg, "Jobs and economic development impact (jedi) model geothermal user reference guide," 9 2012.

[52] P. Yin and Y. Hou, "Dynamic study on particle throwing motion of pulsating negative pressure shale shaker," *Journal of Petroleum Exploration and Production Technology*, vol. 13, pp. 753–762, 11 2022.

[53] J. Jivraj, "Penscriptive depth-controlled robotic laser osteotomy," 5 2021.

[54] E. D. Mattson and L. Hull, "Documentation of inl's in situ oil shale retorting water usage system dynamics model," 12 2012.

[55] M. J. Kieba and C. J. Ziolkowski, "Differential soil impedance obstacle detection," 6 2004.

[56] C. Matteo, P. Candido, R. R. Vera, and V. Francesca, "Current and future nanotech applications in the oil industry," *American Journal of Applied Sciences*, vol. 9, pp. 784–793, 6 2012.

[57] L. Liu, D. Zhan, D. Spencer, and D. Molyneux, "Pack ice forces on floating offshore oil and gas exploration systems," in *SNAME 9th International Conference and Exhibition on Performance of Ships and Structures in Ice*, SNAME, 9 2010.

[58] A. T. Fischer, T. Tsuji, K. Petronotis, C. G. Wheat, K. Becker, J. F. Clark, J. Cowen, K. Edwards, and H. Jannasch, "Iodp expedition 327 and <i>atlantis</i> expedition at 18-07: Observatories and experiments on the eastern flank of the juan de fuca ridge," *Scientific Drilling*, vol. 13, pp. 4–11, 4 2012.

[59] A. S. Apaleke, A. Al-Majed, and M. E. Hossain, “State of the art and future trend of drilling fluid: An experimental study,” in *SPE Latin America and Caribbean Petroleum Engineering Conference*, SPE, 4 2012.

[60] S. Bertram-Howery and P. Swift, “Potential for long-term isolation by the waste isolation pilot plant disposal system,” 6 1990.